PNAS RESEARCH ARTICLE | APPLIED BIOLOGICAL SCIENCES ENGINEERING OPEN ACCESS

An engineered model of metastatic colonization of human bone marrow reveals breast cancer cell remodeling of the hematopoietic niche

Ilaria Baldassarri[a,b,1], Daniel Naveed Tavakol[a,b,1], Pamela L. Graney[a,b], Alan G. Chramiec[a], Hanina Hibshoosh[b,c], and Gordana Vunjak-Novakovic[a,b,d,e,2]

Affiliations are included on p. 9.

Edited by Robert Langer, Massachusetts Institute of Technology, Cambridge, MA; received March 19, 2024; accepted August 16, 2024

Incomplete understanding of metastatic disease mechanisms continues to hinder effective treatment of cancer. Despite remarkable advancements toward the identification of druggable targets, treatment options for patients in remission following primary tumor resection remain limited. Bioengineered human tissue models of metastatic sites capable of recreating the physiologically relevant milieu of metastatic colonization may strengthen our grasp of cancer progression and contribute to the development of effective therapeutic strategies. We report the use of an engineered tissue model of human bone marrow (eBM) to identify microenvironmental cues regulating cancer cell proliferation and to investigate how triple-negative breast cancer (TNBC) cell lines influence hematopoiesis. Notably, individual stromal components of the bone marrow niche (osteoblasts, endothelial cells, and mesenchymal stem/stromal cells) were each critical for regulating tumor cell quiescence and proliferation in the three-dimensional eBM niche. We found that hematopoietic stem and progenitor cells (HSPCs) impacted TNBC cell growth and responded to cancer cell presence with a shift of HSPCs ($CD34^+CD38^-$) to downstream myeloid lineages ($CD11b^+CD14^+$). To account for tumor heterogeneity and show proof-of-concept ability for patient-specific studies, we demonstrate that patient-derived tumor organoids survive and proliferate in the eBM, resulting in distinct shifts in myelopoiesis that are similar to those observed for aggressively metastatic cell lines. We envision that this human tissue model will facilitate studies of niche-specific metastatic progression and individualized responses to treatment.

tissue engineering | metastasis | hematopoiesis | cancer | organoids

Significance

Metastatic disease remains the most significant cause of mortality in cancer patients, due in part to the lack of model systems capable of recapitulating human, patient-specific effects of metastasis. Disseminated cancer cells find microenvironmental niches that support their survival after treatment, leading to recurrence of disease later in life. We report the development of an engineered model of breast cancer (BC) colonization of human bone marrow (BM), allowing for the dissection of niche components that sustain tumor cell adaptation and characterization of blood and immune cell responses to cancer invasion. Further, we demonstrate utility of this model for studying the growth of primary patient-derived BC organoids within the BM niche, providing a unique personalized model of secondary metastatic colonization.

Metastasis is a highly complex, multistep process. Already prior to the homing of circulating tumor cells (CTCs), the primary tumor induces local and systemic changes that lead to the establishment of premetastatic niches (1). Single and clustered CTCs then colonize distant organs, going through a period of quiescence and survival, before propagating into micrometastases (2). Metastatic dissemination can occur even before the primary tumor is detectable, with early disseminated tumor cells (DTCs) that have the potential to recur 5 to 10 y later (3). This phenomenon, known as minimal residual disease, has been associated with tumor dormancy that is driven by a balance of steady-state proliferation and death of cancer cells, which are in turn due to angiogenic impairment, immune pruning, or cellular dormancy (4–9).

The crucial role of the microenvironment in determining DTC phenotype is supported by numerous studies recently reviewed by Lim and Ghajar (10). Advances in our understanding of tumor biology are further complicated by inter-patient and intra-tumor variability, especially in highly aggressive cancers without effective interventional measures for targeting DTCs at secondary metastatic sites. The 5-y survival rate of only 30% following the spread of breast cancer (BC) to distant organs reflects inadequate therapeutic responses (11, 12). Critically, bone is the most common site of BC metastasis (13), with the presence of DTCs in bone marrow (BM) aspirates correlating with poor clinical outcomes (14). The clinical picture is further complicated by cancer cells hijacking the BM niche to promote altered hematopoietic programs at the hematopoietic stem and progenitor cell (HSPC) level. This subversion of hematopoiesis is known as emergency myelopoiesis and has systemic effects on promoting a protumorigenic and premetastatic environment (15), highlighting the need for robust models that can lead to better understanding of complex interactions between DTCs and the hematopoietic-stromal microenvironment.

Over the past decade, bioengineered models of cancer have emerged to complement traditional preclinical models of metastasis, offering new versatile tools for studying the metastatic

Author contributions: I.B., D.N.T., and G.V.-N. designed research; I.B., D.N.T., P.L.G., and A.G.C. performed research; I.B., D.N.T., and H.H. analyzed data; and I.B., D.N.T., and G.V.-N. wrote the paper.

Competing interest statement: D.N.T., P.L.G., and G.V.-N. have filed patent application for technology utilized in this research, through Columbia University.

This article is a PNAS Direct Submission.

[1]I.B. and D.N.T. contributed equally to this work.

[2]To whom correspondence may be addressed. Email: gv2131@columbia.edu.

This article contains supporting information online at https://www.pnas.org/lookup/suppl/doi:10.1073/pnas.2405257121/-/DCSupplemental.

Published October 7, 2024.

process and identifying druggable targets for clinical translation (16–18). Organs-on-a-chip (OOC), also known as microphysiological systems, are in vitro human tissue models that can be tailored to emulate individual aspects of tissue and organ functions (19, 20). In recent years, these models have started to serve as platforms for investigating metastatic disease and its treatment within controlled and physiologically relevant settings (17, 21–26). The complexity of an OOC is dictated by the proposed research question, with flexibility to enable the deconstruction of microenvironmental and cellular contributions to cancer progression (16, 17, 20, 21, 27). The field has also reported the value of simple in vitro models for the identification of drivers of dormancy and reactivation (28). Foundational studies by Ghajar et al. demonstrated the use of bioengineered organotypic models of vasculature to investigate the induction of dormancy (29). More recently, fibronectin deposition and degradation were shown to alter DTC cell cycle in BM, using cancer cell lines cultured on extracellular matrix (ECM) substrates with tunable composition (30). The growth-restrictive nature of the BM niche has made it a focus of numerous studies of cancer dormancy, with several parallels drawn between stromal cues that regulate the behaviors of HSPCs and DTCs (9, 10, 31, 32).

Significant progress has been made in the development of human BM models with three-dimensional (3D) architecture capable of hematopoietic function (33–39). In 2018, Bourgine et al. described the first entirely human, perfused BM niche, built on ceramic scaffolds lined with osteoblasts (OBs) (37). In recent studies, Glaser et al. engineered a microfluidic, multi-niche human BM model apt for studies of selective migration of cancer cells toward endosteal or perivascular niches (38), whereas Khan et al. generated BM organoids with myelopoietic function that partially recapitulated the stromal milieu of the niche for studying cancer-stroma interactions in blood malignancies (39). These findings build the collective foundation for early assessment of metastatic risk, enabling more effective individualized therapies, and driving innovation of bioengineered BM models (16, 17, 40). However, the lack of human BM models that incorporate both hematopoiesis and metastatic cancer cells limits the capability to demonstrate metastatic invasion of the BM and the ensuing alterations to BM hematopoiesis.

Here, we report the development of an engineered human BM model of BC colonization. Using a combination of primary OBs, endothelial cells (ECs), and mesenchymal stem/stromal cells (MSCs), we identified stroma-driven cues regulating homing of metastatic BC cells to the niche. This approach enabled the investigation of secondary tumor cell proliferation and of the remodeling of a metastatic target organ harboring disseminated cells that can persist and grow after therapeutic interventions. By inclusion of cord blood-derived HSPCs (CB-HSPCs), with and without metastatic BC cells, we studied the blood cell production and emergency myelopoiesis involved in metastatic invasion, and the cross-talk between resident and cancer cell types. Finally, we engrafted patient-derived BC organoids into the BM tissue model, as a proof-of-concept for assessing individualized responses in a metastatic site in vitro. In these studies, we started to look into the potential mechanisms driving cancer cell behavior and established a model for controlled patient-specific studies of BM-tumor cell interactions.

Results

Engineering a Human Model of Metastatic Colonization of Bone Marrow. In our previously established model of the human BM (eBM), an endosteal niche interfaces with a perivascular region enriched with a hematopoietic population (41, 42). This endosteal niche is created by seeding and expanding primary BM-derived MSCs into decellularized bone scaffolds, followed by their differentiation into OBs over a period of 3 wk under osteogenic conditions. Once the engineered bone is fully developed, the perivascular niche in the healthy eBM is established by seeding MSCs, ECs, and CB-HSPCs within a fibrin hydrogel. Here, by leveraging the diverse cellular composition of the perivascular compartment, BC cells were incorporated into the fibrin matrix to simulate the evolution of DTCs homing to the marrow. Cancer cells were initially seeded as single-cell suspensions, whereas later studies that incorporated patient-derived tumor organoids relied on their fragmentation prior to seeding. The resulting tissues were cultured for up to two additional weeks and subjected to histological, flow cytometric, and proteomic analyses (Fig. 1*A*).

First, we investigated whether triple-negative breast cancer (TNBC) MDA-MB-231 cells labelled with GFP could be maintained in the eBM niche for extended periods of time, and probed tissue-level changes occurring to the eBM as the niche was overtaken. Histological analysis confirmed the presence of GFP^+ MDA-MB-231 cells in the perivascular region of the eBM both in hematoxylin and eosin (H&E) and immunofluorescence (IF) staining. In particular, over 2 wk of integrated culture, colonized eBM tissues contained visibly less $CD45^+$ cells in the adherent cell fraction. $CD31^+$ vascular networks were noticeably disrupted compared to controls as malignant growth progressed (Fig. 1 *B* and *C*). Following tissue digestion, the impact of cancer cell presence on immune cell maintenance and expansion was further characterized by flow cytometry. Consistent with qualitative observations, the percentage of adherent $CD45^+$ cells in eBM was vastly reduced in tissues seeded with MDA-MB-231. The concomitant reduction in the count of adherent $CD45^+$ blood cells compared to the healthy eBM suggested that malignant cells were directly affecting the expansion potential of immune cells (Fig. 1*D*).

Among the tissue-level changes that occur with metastatic colonization, we set to characterize changes to the ECM of invaded eBM tissues. To this end, we snap-froze and decellularized the tissues and performed proteomic analysis to detect the significantly up- and down-regulated proteins associated with stromal cell support. Notably, numerous matrix-associated proteins, including COL6A3, had elevated expression levels in colonized eBM tissues compared to healthy controls, whereas the expression of some hematopoietic stromal support factors like CXCL12 decreased (*SI Appendix*, Fig. S1 *A* and *B*). Gene ontology (GO) pathway analysis helped correlate the protein-level changes with the reorganization of collagen within the tissues over 2 wk of integrated culture (*SI Appendix*, Fig. S1*C*).

Stromal Contributions to Metastatic Cancer Cell Survival and Cycling. Cellular components of the endosteal and perivascular BM microenvironment are known to provide biochemical and biophysical cues that influence the stemness and differentiation capacity of HSPCs (43–45). To draw parallels between the maintenance of HSPCs and disseminated cells in the eBM, we delved into the effects of OBs, ECs, and MSCs, key components of the stromal microenvironment of the eBM, on cancer cell behavior.

To this end, we first compared the transcriptomic changes to MDA-MB-231 cancer cells cultured on either endosteal bone (i.e., containing exclusively OBs) or endosteal bone seeded with MSCs and ECs (ME) to form a perivascular niche (Fig. 2*A*). Malignant cells were seeded at a very low density (i.e., 5'000 cells per tissue) to mimic the sparsity of DTCs homing to the marrow following extravasation. After 10 d of culture, we performed bulk RNA sequencing of MDA-MB-231 cancer cells sorted from the multicellular cultures based on the endogenous reporter tdTomato. We

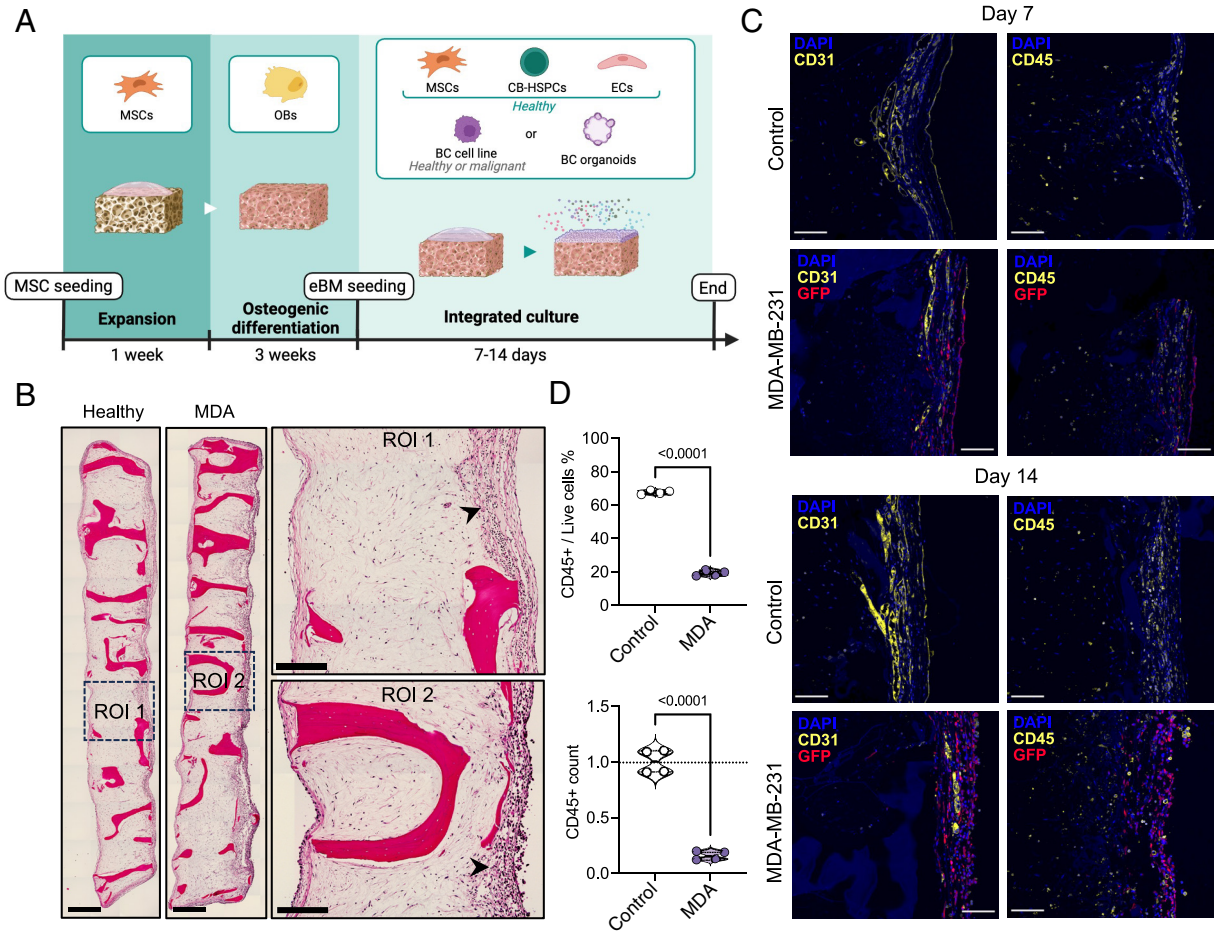

Fig. 1. eBM tissue enables modeling of metastatic BC colonization. (*A*) Methods for generating eBM in integrated culture with BC cell lines or patient-derived organoids for up to 2 wk of 3D coculture. (*B*) Representative H&E staining of the healthy and MDA-colonized eBM tissue sections (Scale bar: 500 μm.) Magnified view of ROIs showcasing interfaces of perivascular-like regions (arrowheads) and endosteal regions (Scale bar: 200 μm.) (*C*) Representative images of the temporal changes in cellular composition in healthy and colonized eBM tissues (Scale bar: 100 μm.) (*D*) Percentages and counts (normalized to control) of CD45+ blood cells in adherent fractions of eBMs following MDA colonization. *P* values determined by two-tailed unpaired *t* test.

identified 116 differentially expressed genes ($P_{adj} < 0.05$, $|\log_2 FC| > 0.2$) between cancer cells isolated from the OB and ME groups to get insights into the roles of ECs and MSCs in harboring a unique BM stromal environment for the malignant cancer cells (Fig. 2 *B–D*). By performing gene set enrichment analysis (GSEA), we identified a number of significantly upregulated pathways associated with cancer cells cultured in ME tissues as compared to those in the OB group. Detected changes included increases in ECM-receptor interactions, collagen formation, unfolded protein response, and hypoxia. Conversely, cells in the ME group had downregulated pathways associated with cell cycle and apoptosis, indicative of a more proliferative phenotype in the OB groups (Fig. 2 *E* and *F*). Normalized enrichment scores (NES) were matched to the increased GO pathways associated with cell migration, cell proliferation, and ECM organization, among others (Fig. 2*G*).

Having identified the critical impact of ECs and MSCs on cancer cell adaptation to the cellular architecture of the eBM, we proceeded to systematically vary its cellular components (i.e., OBs, ECs, MSCs, and CB-HSPCs) to discern their individual and interactive impact on cancer growth. We therefore designed an "N-1" study to progressively incorporate OBs alone, followed by the addition of the perivascular niche, using ECs alone, MSCs alone, a combination of both, and ultimately integrating the functional unit of the eBM, represented by CB-HSPCs (Fig. 2*H*). To quantify cancer cell cycling at the whole-tissue level by flow cytometric analysis, we used the mVenus-p27K$^-$ cell-cycle reporter in MDA-MB-231 cells endogenously tagged with tdTomato (Fig. 2 *H* and *I* and *SI Appendix*, Fig. S2) (46, 47). We recorded the highest counts of tdTomato$^+$ cells in purely endosteal tissues, followed by the tissue infused with MSCs, whereas the eBM model containing all cell types harbored the fewest cancer cells (Fig. 2*I*). Remarkably, the presence of ECs was associated with reduced tdTomato$^+$ counts (Fig. 2*I*). We confirmed that EC networks were not compromised in any of the tissue groups, albeit observing the greatest vascular interconnection in the presence of MSCs compared to ECs only (*SI Appendix*, Fig. S3). Using the mVenus reporter of p27 expression, we observed the lowest percentage of mVenus$^+$ quiescent cells in the eBM tissues (Fig. 2*I*). This finding was in contrast with low tdTomato$^+$ cell counts, suggesting that the hematopoietic compartment of eBM was pruning the cancer cells or suppressing their proliferation without clear induction of p27-mediated cellular quiescence. The remaining trends of mVenus expression were instead in line with those of tdTomato across experimental groups (Fig. 2*I*) and were mirrored in tissue constructs stained for p27 (Fig. 2*J*).

Changes in Hematopoiesis over 2 Wk of Culture with Metastatic Cells. Pathological conditions, including cancer, are known to alter hematopoietic output in what is known as emergency

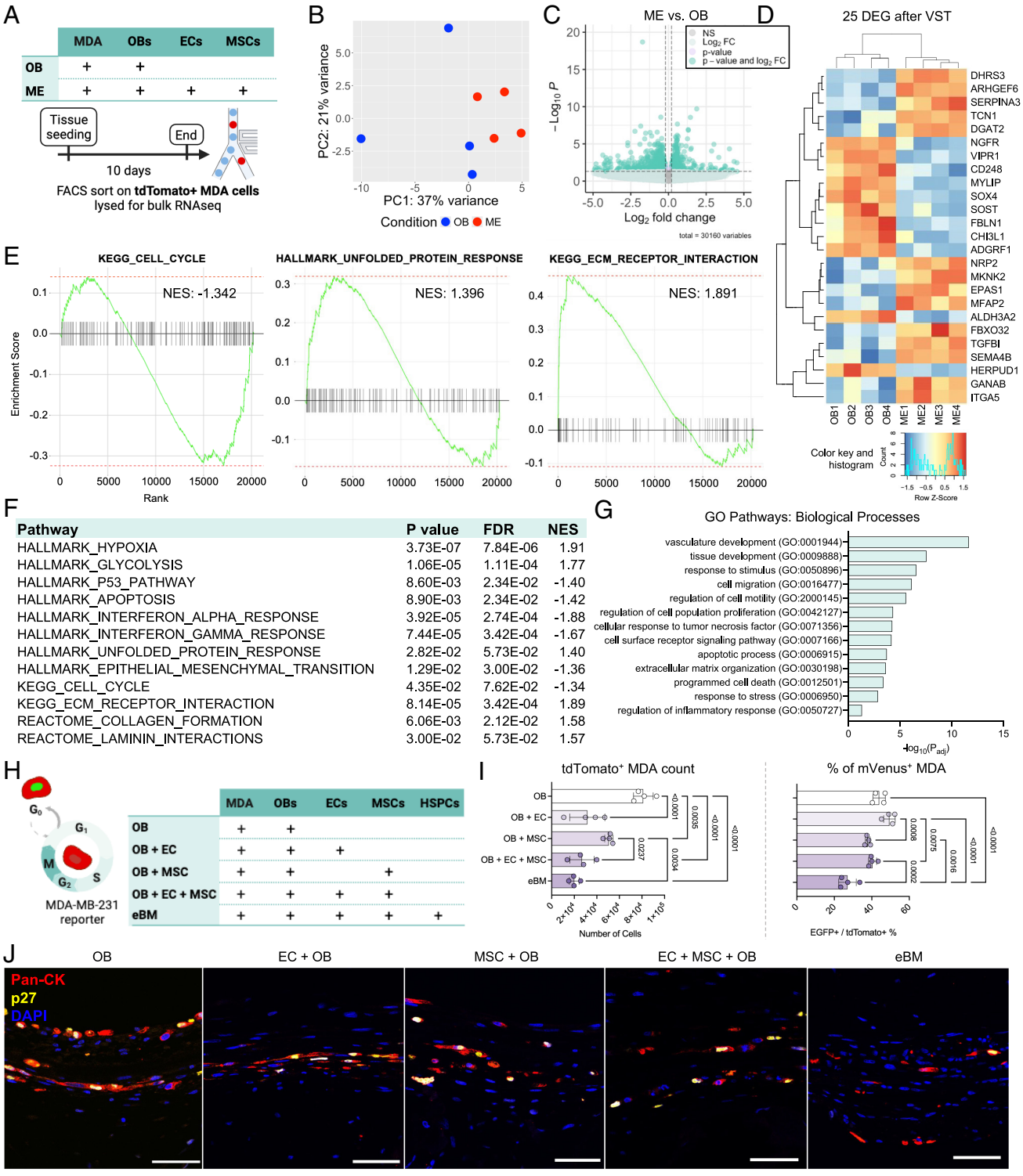

Fig. 2. Stromal factors in eBM tissue model influence adaptation of MDA-MB-231 cells. (*A*) Schematic of the approach adopted to assess the influence of different stromal components of eBM tissues on MDA-MB-231 cell cycling over 10 d of integrated culture. (*B–D*) Principal component analysis (*B*), volcano plot (*C*), and top 25 differentially expressed genes (*D*) in MDA-MB-231 cells isolated from cocultures with OBs, MSCs, and ECs, vs. only OBs alone. (*E* and *F*) Select GSEA in differentially expressed genes for the above comparisons. (*G*) Select relevant GO pathway analysis for biological processes implicated in the above differentially expressed genes (MDA-MB-231 cells isolated from ME vs. OB cultures). (*H*) Schematic of the "N-1" approach used to assess niche cues regulating tumor cell cycling via flow cytometry using a tdTomato-mVenus-p27K$^-$ reporter. (*I*) Quantification of total tdTomato$^+$ MDA-MB-231 cells and percentage of quiescent mVenus$^+$ MDA-MB-231 cells at 10 d of coculture. *P* values determined by ordinary one-way ANOVA with Tukey's multiple comparison test. (*J*) Representative images of MDA-MB-231 cells (pan-CK, red) stained for the quiescence marker p27 (yellow) in coculture with stromal components of the niche. (Scale bar: 50 μm.)

myelopoiesis (48, 49). Prior to investigating the ability of the eBM to capture this phenomenon, we characterized the changes in hematopoietic lineages and differentiation capacity of CB-HSPCs in the presence of metastatic cancer cell lines. To this end, we cocultured MDA-MB-231 and its in vivo-derived bone-targeting daughter cell line MDA-231-BoM-1833 (50) with CB-HSPCs for 5 d, and assessed hematopoietic progenitor and downstream myeloid cell changes. Via flow cytometry, we identified clear differences between progenitor cell populations in cancer cell fractions (*SI Appendix*, Fig. S4). The fractions of multipotent

$CD34^+CD38^-$ progenitors decreased substantially ($P < 0.001$) in the presence of cancer cells (*SI Appendix*, Fig. S4). Conversely, there were significant increases ($P < 0.001$) in the fractions of $CD11b^+$ and $CD11b^+CD14^+$ myeloid cells between all coculture groups and controls (*SI Appendix*, Fig. S4). Interestingly, bone-targeting metastatic cells showed the greatest deviation from the control for both the progenitor and myeloid cell differentiation populations (*SI Appendix*, Fig. S4).

In light of these findings, we proceeded to investigate alterations to hematopoiesis in the 3D multicellular architecture of the eBM. To this end, we seeded the eBM with CB-HSPCs at a 1:1 ratio with either MDA-MB-231 or MCF10A cells, representing malignant and benign breast epithelial cells, respectively. To characterize the downstream immune progenies compared to control, we performed flow cytometry on the adherent and suspension cell fractions of eBM tissues (Fig. 3*A* and *SI Appendix*, Fig. S5). After 2 wk of integrated culture, $CD34^+$ progenitors in tissues colonized by MDA-MB-231 followed a decreasing, though not statistically significant, trend. In contrast, we detected significant decreases in percentages of $CD34^+CD38^-CD45RA^-$ multipotent progenitor (MPP) populations in eBM tissues cultured with MDA-MB-231 ($P = 0.0353$) (Fig. 3*B*). These decreases were mirrored by increases in $CD38^+$ expression of $CD34^+$ progenitors in MDA-MB-231 groups ($P = 0.0316$), indicating a shift in the remaining progenitors toward a more committed myeloid phenotype among $CD34^+CD38^+CD45RA^-$ common myeloid progenitors (CMPs; $P = 0.0331$). Notably, there were no changes associated with the presence of benign epithelial cells in eBM tissues (Fig. 3*B*).

MDA-MB-231-colonized eBMs demonstrated increased percentages of $CD33^+$ myeloid ($P < 0.0001$) and $CD71^+$ myelo-erythroid ($P = 0.004$) lineages (Fig. 3*C*). Evaluation of the myeloid fractions of $CD45^+$ blood cells showed a detectable side scatter shift in $CD11b^+$ total myeloid cells and $CD14^+$ monocytes in MDA-MB-231-colonized eBMs, indicating increased myeloid cell differentiation toward mature progeny (i.e., monocytes and macrophages) (Fig. 3 *D*–*G*). Quantification revealed significant increases in percentages of $CD11b^+$ myeloid cells ($P < 0.0001$) and $CD14^+$ monocytes ($P = 0.0001$) for MDA-MB-231 groups (Fig. 3 *D*–*G*). $CD68^+$ macrophages were found to infiltrate MDA-MB-231 metastatic pockets in the eBM (Fig. 3*H*). Increases in numbers of myeloid progeny correlated with increases in $CD14^+CD11c^+$ dendritic-like cell numbers ($P = 0.0002$), and decreases in numbers of maturing $CD14^-CD16^+CD13^+$ granulocytes ($P = 0.0285$) in the myeloid fraction of MDA-MB-231-seeded eBMs (Fig. 3*I*).

We confirmed these findings using two additional cell lines in 3D eBM tissues: the highly metastatic BoM-1833 and the slower-growing T47D hormone receptor positive (HR^+) line (*SI Appendix*, Fig. S6). As seen in monolayer cocultures (*SI Appendix*, Fig. S4), BoM-1833-colonized eBMs also exhibited marked increases in suspension cell percentages of $CD11b^+$ myeloid cells ($P = 0.0001$) and $CD14^+$ monocytes ($P = 0.0001$), as well as decreases in $CD66b^+$ granulocytes ($P = 0.0128$), compared to controls. However, this myelopoietic skewing effect was not evident in the HR^+ T47D line, potentially due to the slower growth rate of these tumor cells in vitro.

Patient-Specific Model of BC Bone Metastasis. To extend the eBM model of metastasis to studies of primary patient tumors, we derived BC organoids (BCOs) from the primary tumors of multiple HR^+ and TNBC patients harvested at diagnosis using established protocols (51). BCOs were derived from the cells of each patient and integrated into the eBM model (Fig. 4 *A*–*D* and *SI Appendix*, Fig. S7). Notably, BCOs preserved the original structure, either dense or cystic, as micrometastases in the perivascular compartment of eBM tissues (Fig. 4*D* and *SI Appendix*, Fig. S7*C*).

All original patient tumor samples were analyzed for immunohistochemical (IHC) expression of canonical molecular BC markers (i.e., estrogen receptor, ER, progesterone receptor, PR, and human epidermal growth factor receptor 2, HER-2) and proliferative capacity (*SI Appendix*, Figs. S7*B* and S8). eBM tissue-adapted BCO1 organoids (see *SI Appendix*, Figs. S7*B* for labeling strategy) underwent analogous characterization, showing a similar lack of ER, PR, and HER-2 expression compared to the respective tumor resections (Fig. 4*D*). Marker of breast tissue origin TRPS1 (52) and TN marker SOX10 (seen in 50% of TN carcinomas) (53) were positive (Fig. 4*D*). We further characterized the presence of BCOs within eBM, and their interactions with the healthy cell populations in the niche for multiple patients. IF staining demonstrated the presence of $CD45^+$ blood cells and $CD31^+$ ECs surrounding BCOs in the niche, with formation of $CD31^+$ vessel-like structures adjacent to the tumor cells (Fig. 4*E* and *SI Appendix*, Fig. S9). Among $EpCam^+$ cells, cell cycle markers Ki-67 and p27 were heterogeneously expressed (Fig. 4*E* and *SI Appendix*, Fig. S9), congruently with original tissue expression (*SI Appendix*, Fig. S7*B* and Fig. S8).

When isolating the hematopoietic and BC cells from the eBM tissues at endpoint, we noticed distinct scatters separating the $EpCam^+$ tumor cells and $CD45^+$ blood cells (Fig. 5*A* and *SI Appendix*, Fig. S10*A*). We cultured BCOs derived from five patients within the eBMs, resulting in varying $EpCam^+$ ranges associated with the expansion of BCOs upon isolation from resected tissue. For analysis of hematopoietic differentiation trajectories, we chose the most proliferative line (BCO4) with an $EpCam^+$ percentage of ~20% in the adherent cell fraction of eBMs (Fig. 5*B*). The slight reduction of $CD45^+$ cells (Fig. 5*C*) was in line with the increased $EpCam^+$ tumor cell percentages. In addition, we noticed significant increases in $CD11b^+$ myeloid cells ($P = 0.0054$), $CD14^+$ cells ($P = 0.056$), and $CD66b^+$ cells ($P = 0.0046$) in the adherent cell fractions of BCO4-colonized eBMs (Fig. 5*D*). Increased $CD66b^+$ percentages in the adherent cell fractions (Fig. 5*E*) were not observed in the corresponding cultures of MDA-MB-231 cells (*SI Appendix*, Fig. S6). Notably, there were no significant increases in $CD11b^+$ or $CD14^+$ myeloid cells in suspension fractions; however, the CD66b+ increase in suspension was matched by a decrease in $CD11c^+CD14^+$ dendritic-like cells (Fig. 5*F*).

By culturing another tumor population (i.e., BCO1) within eBM tissues at a lower density, constituting approximately 2.5% of the total adherent cell fraction by flow cytometry at d 7 (*SI Appendix*, Fig. S10*A*), we observed that presence of BCOs from this particular donor did not significantly impact the extent of myelopoiesis or the trajectory of eBM cultures (*SI Appendix*, Fig. S10). Nevertheless, upon a closer look at the mean fluorescence intensity of hematopoietic surface antigens, we detected significant decreases in $CD34^+$ expression and significant increases in $CD11b^+$ and $CD71^+$ myeloid markers (*SI Appendix*, Fig. S10 *B*–*E*).

Discussion

We report a unique approach to examining changes in the BM niche upon its metastatic colonization by BC cell lines and patient-derived tumor cells. The eBM model provides a human stromal microenvironment that supports diverse cancer cell phenotypes and enables detection of changes in hematopoietic differentiation trajectories upon malignant invasion. We thereby demonstrate its ability to reveal niche-specific effects on tumor cell proliferation and to provide durable support of patient-derived organoids. We expect that

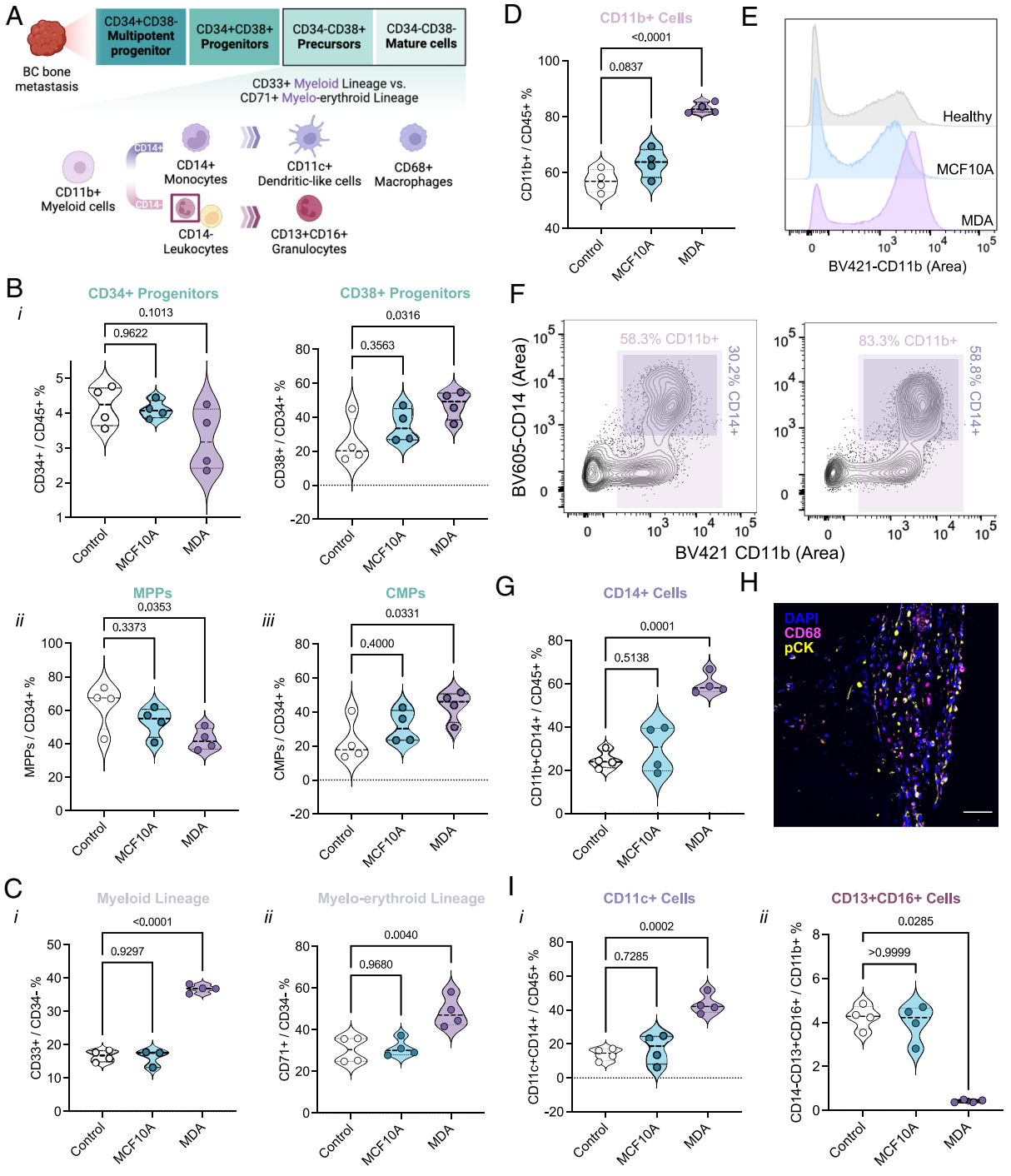

Fig. 3. MDA-MB-231 cells colonize eBM tissues over 2 wk of integrated culture and induce myeloid skewing of HSPCs. (*A*) Schematic of HSPC downstream differentiation trajectories in eBM and associated markers. (*B*) Percentages of $CD34^+$ (*Left*) and $CD38^+$ progenitors (*Right*), *i*, MPPs, *ii*, and CMPs, *iii*. (*C*) Percentages of $CD33^+$ myeloid lineage cells, *i*, and $CD71^+$ myelo-erythroid progeny, *ii*, in the suspension fraction of eBMs. (*D*) $CD11b^+$ cell percentages in the suspension fraction of eBMs. (*E*) Representative shifts in CD11b expression levels. (*F*) Representative flow cytometry gating of healthy and colonized eBM tissues with increased CD11b and CD14 expression levels. (*G*) $CD14^+$ cell percentages in the suspension fraction of eBMs. (*H*) Representative image of macrophage infiltration in metastatic pockets in the eBM (Scale bar: 50 μm.) (*I*) Changes in suspension percentages of $CD11c^+$ dendritic-like cells, *i*, and mature $CD13^+$ granulocytes, *ii*. *P* values determined by ordinary one-way ANOVA with Dunnet's multiple comparison test or Kruskal-Wallis test with Dunn's multiple comparisons.

our findings will enable the use of the eBM model to identify factors of the niche hindering efficacious therapeutic interventions and improve outcomes by exploiting its human, patient-specific nature.

Over the last decade, several studies have documented the critical role of the microenvironment in modulating cancer cell proliferation, both in vitro and in vivo. The BM niche is known to be growth restrictive, and a multitude of mechanisms driving cellular dormancy of DTCs has been identified (9). Although animal models have unlocked a realm of therapeutic interventions, human tissue models are critical for evaluating the contributions of stromal cell populations to cancer cell behavior. We show that the human eBM model provides versatile cellular compositions in its microenvironment with a concerted impact on cancer cell cycling that can be parsed out by selective inclusion of constituent stromal cells using both transcriptomic analysis and reporters tailored to monitoring cell quiescence. To this

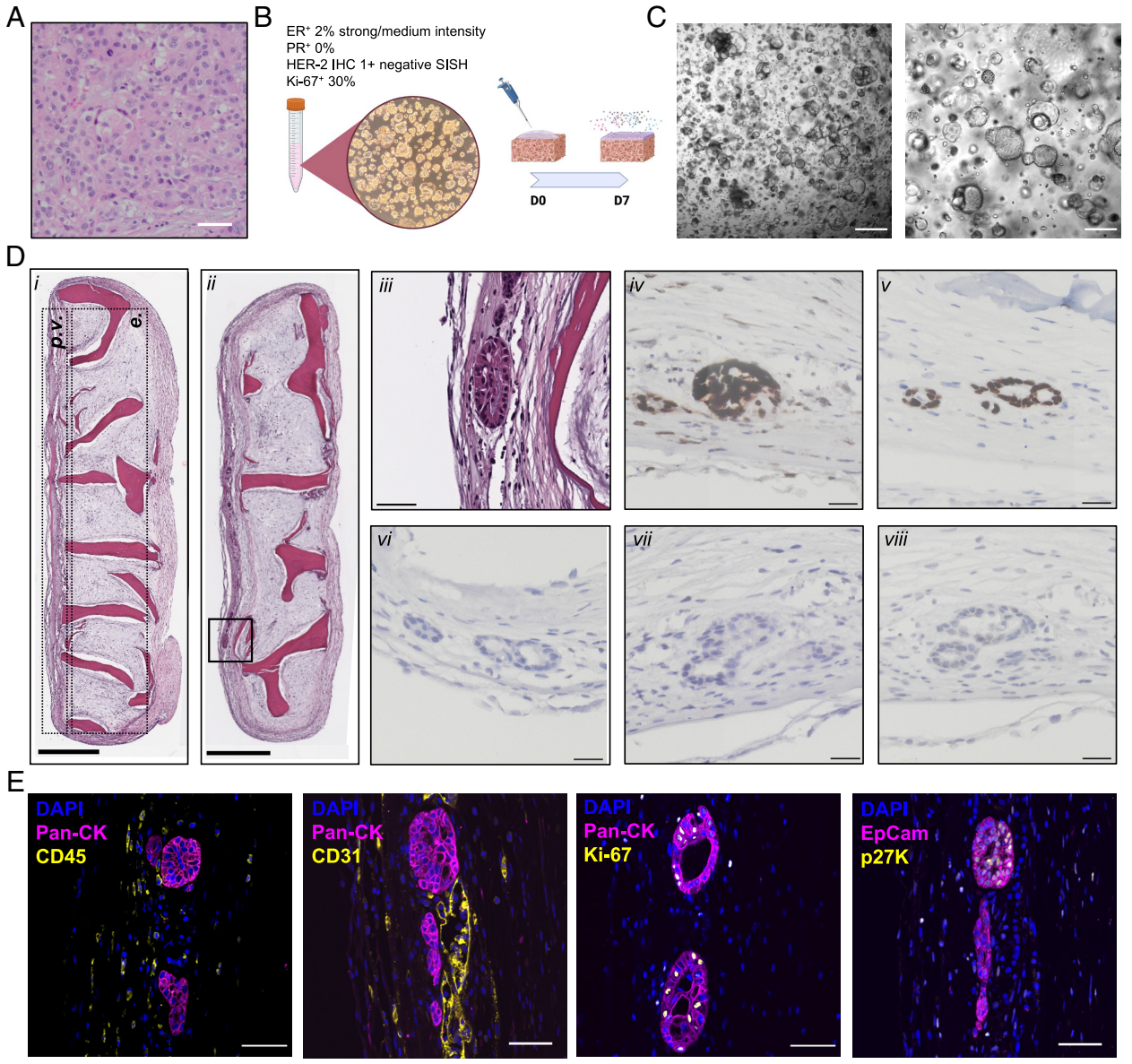

Fig. 4. Patient-derived organoids integrate into the eBM model. (*A*) H&E of the original tumor sample (Scale bar: 50 μm.) (*B*) Schematic of the approach adopted to embed BCOs into the eBM for 7 d of integrated culture. Representative images of BCOs released from Matrigel using 2 U/mL dispase. (*C*) Representative brightfield images of BCOs embedded in Matrigel domes (Scale bar: 500 μm, *Left*, and 50 μm, *Right*.) (*D*) Representative H&E staining of whole healthy, *i*, and colonized, *ii*, eBM sections showcasing interfacing perivascular, *p.v.*, and endosteal-like, *e.*, regions (Scale bar: 500 μm.) Magnified view on H&E stain displaying a BCO embedded within the perivascular space of the eBM, *iii* (Scale bar: 50 μm.) Representative images of BC-specific IHC staining: TRPS1, *iv*, SOX10, *v*, HER2/Neu, *vi*, PR, *vii*, and ER, *viii* (Scale bar: 25 μm.) (*E*) Immunostaining of organoids at day 7 of integrated culture in the eBM as indicated (Scale bar: 50 μm.)

end, we opted for low-density seeding of dissociated cancer cells, as opposed to cell clusters, to recapitulate the paucity of DTCs homing to BM and the consequent stromal influences. In particular, our model captures to some extent the contributions of ECs to cancer cell growth, in line with the previous reports on dormancy-promoting effects of microvascular networks (29). Heightened interactions of cancer cells with the ECM were detected at the transcriptomic level in the presence of ECs and MSCs compared to OB-only bone tissues, revealing that niche remodeling captured at the proteomic level can at least in part be attributed to these additional cell types. Interestingly, as compared to OB-only tissues, MDA-MB-231 cells from ME tissues (i.e., containing OBs, ECs, and MSCs) were significantly upregulated in genes relating to invasiveness and metastatic potential, including TCN1 and SERPINA3, both of which have been implicated in reduced sensitivity and resistance to therapeutic targeting (54, 55). Interestingly, ITGA5, a prognostic marker of BC-to-bone metastasis, also had significantly increased expression in ME tissues, potentially indicating the ability of the multicellular niche to effectively mimic a metastatic site as compared to solely OBs (56). Our findings further highlight the impact of functional hematopoietic progenitors and immune progeny on disseminated malignant cells, which display significantly lower expression of mVenus-p27K$^-$ and are fewer in number, hinting that immune cells are strongly down-regulating their proliferation despite not activating the cell-cycle reporter used to capture induction of cellular quiescence.

New BM models have emerged to recapitulate hematopoiesis, production of immune cells and altered hematopoietic output during pathological states (i.e., injury, blood disease, infection) (41, 57–59). We previously studied metastatic colonization of vascularized bone without the inclusion of hematopoietic components (60). Recently,

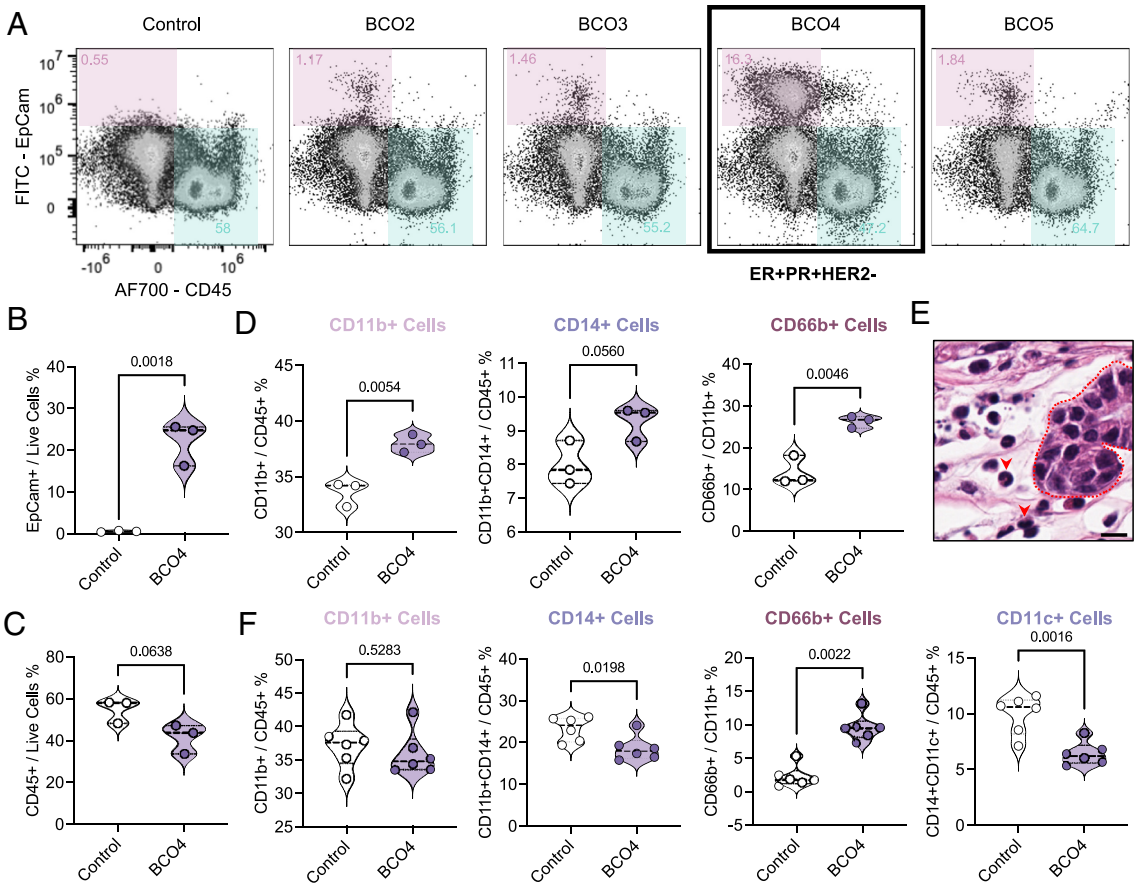

Fig. 5. Patient-derived organoids induce myelopoietic shift when integrated within the 3D eBM model. (*A*) Representative flow cytometry scatters of epithelial (EpCam) and blood/immune (CD45) cells isolated from eBMs after 1 wk of culture for multiple patient donors. (*B* and *C*) BCO4 was subjected to flow cytometric analysis due to large volumes of cells generated from the original tumor sample (~75,000 cells per eBM tissue), corresponding to 20% of the total cell content of the tissue (*B*), while resulting in a slight reduction in total $CD45^+$ cell counts (*C*). (*D*) Percentages of $CD11b^+$, $CD14^+$, and $CD66b^+$ cells in the adherent fractions of the BCO-cultured eBM tissues. (*E*) Representative H&E image of granulocytes (red arrowheads) in the proximity of BCOs (dashed red contour, Scale bar: 10 μm.) (*F*) Percentages of $CD11b^+$, $CD14^+$, $CD66b^+$, or $CD11c^+CD14^+$ cells in the suspension fractions of the BCO-cultured eBM tissues. *P* values determined by two-tailed unpaired t test or Mann–Whitney test.

George et al. demonstrated that metastatic BC cells invade an engineered BM, without analyzing their impact on blood production (38). Our work builds upon these studies to investigate how the blood compartment harbored in the eBM model responds to metastatic invasion. Through culture of cancer cell lines within the eBM, we elucidated downstream changes to immune cell production (i.e., increased myeloid output) and the ECM, which together may reveal unique insights into the protective role of the BM niche. The observed increases in myelopoiesis were corroborated by clinical and animal studies suggesting that the emergency myeloid response can protect DTCs from destruction by immune cells (61, 62).

We also engrafted patient-derived tumor organoids into the engineered BM tissue to overcome limitations of cancer cell lines and account for interpatient and intratumor variability (16, 51, 63, 64), as well as for the presence of stromal factors and human ECM components (65–74). The eBM was utilized as a functional tissue unit responding to cancer cell lines and patient-derived tumor cells. We envision that this model will enable studies of the tumor-niche interactions that control metastatic homing in patient-specific settings, contributing to the identification of therapeutic targets that can halt metastatic progression. In addition, patient-derived metastatic cells within engineered tissue models allow for the incorporation of patient variability into the experimental design to identify commonalities in the resistance or response to therapy.

Our model was able to maintain both quiescent ($p27^+$) and proliferative ($Ki\text{-}67^+$) patient-derived tumor cells and to demonstrate myelopoietic skewing of the eBM, with an increase in granulocytes not found in integrated MDA-MB-231 cultures. These responses are closer to those seen in preclinical animal models and patients, as an increase in granulopoiesis is paralleled by an increase in monocytic myeloid progeny in vivo (75–77). In support of future studies of the feedback loops relating myeloid cell abundance to cancer growth, both macrophages and neutrophils have been reported to impact tumor cell cycling in vivo, for different microenvironments and stages of metastasis (78–80). Despite the promise of our model, its use in conjunction with other cancer cell lines and heterogenous primary tumors will require further optimization and scaling to capture the effects of more and less aggressive cancer cells within the same time frame.

We further acknowledge several limitations of our studies. We investigated metastatic colonization of BM using single-cell suspensions of cancer cell lines and patient-derived organoid fragments seeded sparsely within the perivascular region of the eBM model. In reality, circulating cancer cells selectively extravasate and home into secondary tissues in response to trophic signals (81). While our model captures reciprocal effects of cancer cells on BM stroma and blood cells, it lacks vascular circulation and its known role in DTC entry into the bone through $E\text{-selectin}^+$ gateways (31). A more realistic representation of the metastatic cascade in vitro should involve cancer cell extravasation from the vasculature into the tissues

representing metastatic targets. Notably, Kamm and colleagues have incorporated the extravasation of cancer cells into bone from microfluidic circulation driven by chemoattraction (24), and have later addressed the contribution of circulating monocytes to metastatic efficiency (25).

Our group has engineered bone with vascular perfusion and developed multi-tissue platforms linked by vascular flow that enable selective transport of cells across endothelial barriers, in response to trophic signals (42, 82, 83). Incorporation of perfusion into the eBM would represent an important advance, enabling gain and loss of function studies from early dissemination to late colonization aiming at the identification of elements of the niche that protect cancer cells from therapeutic interventions (84). Furthermore, the eBM model harbors hematopoietic progenitors which can populate vascular channels with immune cells known to orchestrate metastatic progression (42). We believe that this paradigm represents the next generation of engineered models of metastasis (16), where metastatic subsets of cells are selected from a heterogeneous pool of circulating patient-derived tumor cells upon their homing to the niche across the endothelium.

The present study also lacks thorough characterization of the cell types responsible for ECM remodeling and their impact on cancer cell behaviors, as well as the molecular drivers of cancer cell adaptation to the eBM. Finally, we report only a proof-of-concept study of patient-specific metastasis to the BM by engraftment of primary tumor organoids from five patients. Due to the known interpatient and intratumor heterogeneity of primary cancer cells, a much larger patient cohort will be needed for validating personalized medicine approaches.

In summary, we present an engineered human tissue model of metastatic colonization of BM by BC cells and report the changes in blood production and the BM microenvironment during metastatic progression. This model uniquely includes BCOs that enable studies of patient-specific tumor cell survival and adaptation to a tissue niche canonically associated with BC spread and relapse. We believe that these findings may inform therapeutic measures targeting metastatic sites and help assess the changes to the BM during colonization.

Materials and Methods

All eBM tissues were generated by first seeding BM-MSCs (American Type Culture Collection) onto custom decellularized bone scaffolds and exposing cultures to osteogenic media for 3+ wk. After OB maturation, additional BM-MSCs, human umbilical vein ECs (Lonza), and CB-HSPCs (Stem Cell Technologies) were seeded within a fibrin hydrogel on top of the matured endosteal tissues, with or without an additional tumor cell population (i.e., MDA-MB-231 cell line, T47D cell line, or primary BC-derived tumor organoids, among others). eBM tissues colonized with cancer cell lines were maintained with StemSpan™ Serum-Free Expansion Medium II (Stem Cell Technologies) supplemented with 5% heat-inactivated FBS (Corning), 1% P/S (Gibco), selected EGM™-2 Endothelial Cell Growth Medium-2 BulletKit™ (Lonza) components, and 50 ng/mL each of SCF, TPO, and FLT-3L (PeproTech), for up to 14 d. Experiments conducted for characterization of hematopoietic differentiation trajectory were carried out for 14 d, and experiments with primary tumor organoids were performed for 7 d. For all experiments, subsets of eBM tissues were digested with Collagenase II (Worthington) and Nattokinase (Japan BioSciences) for flow cytometry analysis or RNA sequencing, in addition to a subset of tissues being fixed in 4% paraformaldehyde (Sigma) for histological analysis. A detailed description of materials and methods can be found in *SI Appendix*.

Data, Materials, and Software Availability. All study data are available in the article, *SI Appendix*, Figshare (85), GEO GSE277786 (86), and by request from the Principal Investigator.

ACKNOWLEDGMENTS. We gratefully acknowledge the funding support of this work by the NIH (Grants 5R01CA249799, 3UH3EB025765, P41 EB027062, and 1U54CA274506-01A1 to G.V.-N.; National Research Service Award 1F31CA275733 to D.N.T.), Chan Zuckerberg Biohub New York (CZBNY CU24-1583 to G.V.-N.), NSF (Grant GRFP 1644869 to D.N.T.), and the Columbia Biomedical Engineering Kaganov Fellowship (to I.B.). These studies used the Shared Resources of the Herbert Irving Comprehensive Cancer Center at Columbia University, funded in part through the NIH/National Cancer Institute Cancer Center Support Grant P30CA013696. We thank the staff of the Genomics and High Throughput Screening Shared Resource, Dr. Rajesh Soni and the staff of the Proteomics Shared Resource, Dr. Theresa Swayne and the staff of the Confocal and Specialized Microscopy Shared Resource, the Molecular Pathology Shared Resource with support from Kevin Sun, and the Biomedical Informatics Shared Resource with assistance from Dr. Richard Friedman for their technical support. Research presented in this publication utilized the Columbia Stem Cell Initiative Flow Cytometry core facility at Columbia University Irving Medical Center, under the direction of Michael Kissner, supported by the NIH grant S10OD026845. Conditioned media for organoid cultures were graciously provided by Dr. Anil Rustgi and Dr. Ricardo Cruz-Acuña. We gratefully acknowledge the helpful discussions and technical support of Sue Halligan, Dr. Alan Chiu, Dr. Sharon Fleischer, Dr. Elisa Cimetta, Connie Chen, Derek Ning, Dr. Bryan Wang, and Maria Samaritano, and the help of Katherine Cunningham with editing the manuscript.

Author affiliations: [a]Department of Biomedical Engineering, Columbia University, New York, NY 10025; [b]Herbert Irving Comprehensive Cancer Center, Columbia University, New York, NY 10032; [c]Department of Pathology and Cell Biology, Columbia University, New York, NY 10032; [d]Department of Medicine, Columbia University, New York, NY 10032; and [e]College of Dental Medicine, Columbia University, New York, NY 10032

1. H. Peinado *et al.*, Pre-metastatic niches: Organ-specific homes for metastases. *Nat. Rev. Cancer* **17**, 302–317 (2017).
2. F. G. Giancotti, Mechanisms governing metastatic dormancy and reactivation. *Cell* **155**, 750-764 (2013).
3. Y. Hüsemann *et al.*, Systemic spread is an early step in breast cancer. *Cancer Cell* **13**, 58–68 (2008).
4. N. Almog *et al.*, Prolonged dormancy of human liposarcoma is associated with impaired tumor angiogenesis. *FASEB J.* **20**, 947–949 (2006).
5. C. M. Koebel *et al.*, Adaptive immunity maintains occult cancer in an equilibrium state. *Nature* **450**, 903–907 (2007).
6. A. Pommier *et al.*, Unresolved endoplasmic reticulum stress engenders immune-resistant, latent pancreatic cancer metastases. *Science* **360**, eaao4908 (2018).
7. D. Sun *et al.*, MacroH2A impedes metastatic growth by enforcing a discrete dormancy program in disseminated cancer cells. *Sci. Adv.* **8**, eabo0876 (2022).
8. P. Aouad *et al.*, Epithelial-mesenchymal plasticity determines estrogen receptor positive breast cancer dormancy and epithelial reconversion drives recurrence. *Nat. Commun.* **13**, 4975 (2022).
9. E. Risson, A. R. Nobre, V. Maguer-Satta, J. A. Aguirre-Ghiso, The current paradigm and challenges ahead for the dormancy of disseminated tumor cells. *Nat. Cancer* **1**, 672–680 (2020).
10. A. R. Lim, C. M. Ghajar, Thorny ground, rocky soil: Tissue-specific mechanisms of tumor dormancy and relapse. *Semin. Cancer Biol.* **78**, 104–123 (2022).
11. G. P. Gupta, J. Massague, Cancer metastasis: Building a framework. *Cell* **127**, 679–695 (2006).
12. American Cancer Society Medical and Editorial Content Team, Survival Rates for Breast Cancer. American Cancer Society (2024). https://www.cancer.org/. Accessed 19 September 2024.
13. C. S. B. Galasko, Bone metastases studied in experimental animals. *Clin. Orthopaed. Relat. Res.* **155**, 269–285 (1981).
14. S. Braun *et al.*, A pooled analysis of bone marrow micrometastasis in breast cancer. *N. Engl. J. Med.* **353**, 793–802 (2005).
15. J. W. Swann, O. C. Olson, E. Passegué, Made to order: Emergency myelopoiesis and demand-adapted innate immune cell production. *Nat. Rev. Immunol.* **24**, 596–613 (2024).
16. P. L. Graney, D. N. Tavakol, A. Chramiec, K. Ronaldson-Bouchard, G. Vunjak-Novakovic, Engineered models of tumor metastasis with immune cell contributions. *iScience* **24**, 102179 (2021).
17. K. Ronaldson-Bouchard *et al.*, Engineering complexity in human tissue models of cancer. *Adv. Drug. Deliv. Rev.* **184**, 114181 (2022).
18. G. F. Beeghly, K. Y. Amofa, C. Fischbach, S. Kumar, Regulation of tumor invasion by the physical microenvironment: Lessons from breast and brain cancer. *Annu. Rev. Biomed. Eng* **24**, 29–59 (2022).
19. D. E. Ingber, Human organs-on-chips for disease modelling, drug development and personalized medicine. *Nat. Rev. Genet.* **23**, 467–491 (2022).
20. G. Vunjak-Novakovic, K. Ronaldson-Bouchard, M. Radisic, Organs-on-a-chip models for biological research. *Cell* **184**, 4597–4611 (2021).
21. S. Choi *et al.*, Bone-matrix mineralization dampens integrin-mediated mechanosignalling and metastatic progression in breast cancer. *Nat. Biomed. Eng.* **7**, 1455–1472 (2023).

22. X. Ji *et al.*, Premetastatic niche mimicking bone-on-a-chip: A microfluidic platform to study bone metastasis in cancer patients. *Small* **19**, 2207606 (2023).
23. A. Grigoryan *et al.*, Engineering human mini-bones for the standardized modeling of healthy hematopoiesis, leukemia, and solid tumor metastasis. *Sci. Transl. Med.* **14**, eabm6391 (2022).
24. J. S. Jeon *et al.*, Human 3D vascularized organotypic microfluidic assays to study breast cancer cell extravasation. *Proc. Natl. Acad. Sci. U.S.A.* **112**, 214 (2015).
25. A. Boussommier-Calleja *et al.*, The effects of monocytes on tumor cell extravasation in a 3D vascularized microfluidic model. *Biomaterials* **198**, 180–193 (2019).
26. K. Haase, G. S. Offeddu, M. R. Gillrie, R. D. Kamm, Endothelial regulation of drug transport in a 3D vascularized tumor model. *Adv. Funct. Mater.* **30**, 2002444 (2020).
27. L. Ling *et al.*, Obesity-associated adipose stromal cells promote breast cancer invasion through direct cell contact and ECM remodeling. *Adv. Funct. Mater.* **30**, 1910650 (2020).
28. M. Montagner, E. Sahai, In vitro models of breast cancer metastatic dormancy. *Front. Cell Dev. Biol.* **8**, 37 (2020).
29. C. M. Ghajar *et al.*, The perivascular niche regulates breast tumour dormancy. *Nat. Cell Biol.* **15**, 807–817 (2013).
30. L. E. Barney *et al.*, Tumor cell-organized fibronectin maintenance of a dormant breast cancer population. *Sci. Adv.* **6**, eaaz4157 (2020).
31. T. T. Price *et al.*, Dormant breast cancer micrometastases reside in specific bone marrow niches that regulate their transit to and from bone. *Sci. Transl. Med.* **8**, 340ra373 (2016).
32. A. R. Nobre *et al.*, Bone marrow NG2(+)/Nestin(+) mesenchymal stem cells drive DTC dormancy via TGFβ2. *Nat. Cancer* **2**, 327–339 (2021).
33. D. N. Tavakol, S. Fleischer, G. Vunjak-Novakovic, Harnessing organs-on-a-chip to model tissue regeneration. *Cell Stem. Cell* **28**, 993–1015 (2021).
34. D. N. Tavakol *et al.*, Lessons from biology: Engineering design considerations for modeling human hematopoiesis. *Curr. Stem Cell Rep.* **7**, 174–184 (2021).
35. A. E. Gilchrist, B. A. C. Harley, Connecting secretome to hematopoietic stem cell phenotype shifts in an engineered bone marrow niche. *Integr. Biol. (Camb)* **12**, 175–187 (2020).
36. L. E. Jansen *et al.*, A poly(ethylene glycol) three-dimensional bone marrow hydrogel. *Biomaterials* **280**, 121270 (2022).
37. P. E. Bourgine *et al.*, In vitro biomimetic engineering of a human hematopoietic niche with functional properties. *Proc. Natl. Acad. Sci. U.S.A.* **115**, E5688–E5695 (2018).
38. D. E. Glaser *et al.*, Organ-on-a-chip model of vascularized human bone marrow niches. *Biomaterials* **280**, 121245 (2022).
39. A. O. Khan *et al.*, Human bone marrow organoids for disease modeling, discovery, and validation of therapeutic targets in hematologic malignancies. *Cancer Discov.* **13**, 364–385 (2023).
40. D. N. Tavakol *et al.*, Emerging trajectories for next generation tissue engineers. *ACS Biomater. Sci. Eng.* **8**, 4598–4604 (2022).
41. D. N. Tavakol *et al.*, Modeling and countering the effects of cosmic radiation using bioengineered human tissues. *Biomaterials* **301**, 122267 (2023).
42. D. N. Tavakol *et al.*, Modeling the effects of protracted cosmic radiation in a human organ-on-chip platform. *Adv. Sci. (Weinh)* e2401415 (2024), 10.1002/advs.202401415.
43. S. J. Morrison, D. T. Scadden, The bone marrow niche for haematopoietic stem cells. *Nature* **505**, 327–334 (2014).
44. S. Pinho, P. S. Frenette, Haematopoietic stem cell activity and interactions with the niche. *Nat. Rev. Mol. Cell Biol.* **20**, 303–320 (2019).
45. L. Ding, T. L. Saunders, G. Enikolopov, S. J. Morrison, Endothelial and perivascular cells maintain haematopoietic stem cells. *Nature* **481**, 457–462 (2012).
46. A. L. Correia *et al.*, Hepatic stellate cells suppress NK cell-sustained breast cancer dormancy. *Nature* **594**, 566–571 (2021).
47. T. Oki *et al.*, A novel cell-cycle-indicator, mVenus-p27K−, identifies quiescent cells and visualizes G0–G1 transition. *Sci. Rep.* **4**, 4012 (2014).
48. L. Strauss, V. Guarneri, A. Gennari, A. Sica, Implications of metabolism-driven myeloid dysfunctions in cancer therapy. *Cell. Mol. Immunol.* **18**, 829–841 (2021).
49. Y. Gerber-Ferder *et al.*, Breast cancer remotely imposes a myeloid bias on haematopoietic stem cells by reprogramming the bone marrow niche. *Nat. Cell Biol.* **25**, 1736–1745 (2023).
50. A. J. Minn *et al.*, Genes that mediate breast cancer metastasis to lung. *Nature* **436**, 518–524 (2005).
51. N. Sachs *et al.*, A living biobank of breast cancer organoids captures disease heterogeneity. *Cell* **172**, 373–386.e10 (2018).
52. D. Ai *et al.*, TRPS1: A highly sensitive and specific marker for breast carcinoma, especially for triple-negative breast cancer. *Mod. Pathol.* **34**, 710–719 (2021).
53. G. H. Tozbikian, D. L. Zynger, A combination of GATA3 and SOX10 is useful for the diagnosis of metastatic triple-negative breast cancer. *Hum. Pathol.* **85**, 221–227 (2019).
54. Y. Zhang *et al.*, Overexpression of SERPINA3 promotes tumor invasion and migration, epithelial-mesenchymal-transition in triple-negative breast cancer cells. *Breast Cancer* **28**, 859–873 (2021).
55. G. J. Liu *et al.*, High expression of TCN1 is a negative prognostic biomarker and can predict neoadjuvant chemosensitivity of colon cancer. *Sci. Rep.* **10**, 11951 (2020).
56. F. Pantano *et al.*, Integrin alpha5 in human breast cancer is a mediator of bone metastasis and a therapeutic target for the treatment of osteolytic lesions. *Oncogene* **40**, 1284–1299 (2021).
57. D. B. Chou *et al.*, On-chip recapitulation of clinical bone marrow toxicities and patient-specific pathophysiology. *Nat. Biomed. Eng.* **4**, 394–406 (2020).
58. M. R. Nelson *et al.*, A multi-niche microvascularized human bone marrow (hBM) on-a-chip elucidates key roles of the endosteal niche in hBM physiology. *Biomaterials* **270**, 120683 (2021).
59. C. Ma *et al.*, Leukemia-on-a-chip: Dissecting the chemoresistance mechanisms in B cell acute lymphoblastic leukemia bone marrow niche. *Sci. Adv.* **6**, eaba5536 (2020).
60. A. Marturano-Kruik *et al.*, Human bone perivascular niche-on-a-chip for studying metastatic colonization. *Proc. Natl. Acad. Sci. U.S.A.* **115**, 1256–1261 (2018).
61. L. Strauss *et al.*, RORC1 regulates tumor-promoting "emergency" granulo-monocytopoiesis. *Cancer Cell* **28**, 253–269 (2015).
62. C. S. Netherby, S. I. Abrams, Mechanisms overseeing myeloid-derived suppressor cell production in neoplastic disease. *Cancer Immunol. Immunother.* **66**, 989–996 (2017).
63. R. Fisher, L. Pusztai, C. Swanton, Cancer heterogeneity: Implications for targeted therapeutics. *Br. J. Cancer* **108**, 479–485 (2013).
64. G. Ciriello *et al.*, Comprehensive molecular portraits of invasive lobular breast cancer. *Cell* **163**, 506–519 (2015).
65. R. Cruz-Acuña, G. Vunjak-Novakovic, J. A. Burdick, A. K. Rustgi, Emerging technologies provide insights on cancer extracellular matrix biology and therapeutics. *iScience* **24**, 102475 (2021).
66. V. S. Shirure *et al.*, Tumor-on-a-chip platform to investigate progression and drug sensitivity in cell lines and patient-derived organoids. *Lab Chip* **18**, 3687–3702 (2018).
67. N. Del Piccolo *et al.*, Tumor-on-chip modeling of organ-specific cancer and metastasis. *Adv. Drug Deliv. Rev.* **175**, 113798 (2021).
68. Y. Bi *et al.*, Tumor-on-a-chip platform to interrogate the role of macrophages in tumor progression. *Integrat. Biol.* **12**, 221–232 (2020).
69. J. T. C. Lim *et al.*, Hepatocellular carcinoma organoid co-cultures mimic angiocrine crosstalk to generate inflammatory tumor microenvironment. *Biomaterials* **284**, 121527 (2022).
70. B. Palikuqi *et al.*, Adaptable haemodynamic endothelial cells for organogenesis and tumorigenesis. *Nature* **585**, 426–432 (2020).
71. C. R. Below *et al.*, A microenvironment-inspired synthetic three-dimensional model for pancreatic ductal adenocarcinoma organoids. *Nat. Mater.* **21**, 110–119 (2022).
72. B. L. LeSavage, R. A. Suhar, N. Broguiere, M. P. Lutolf, S. C. Heilshorn, Next-generation cancer organoids. *Nat. Mater.* **21**, 143–159 (2022).
73. R. Cruz-Acuña *et al.*, Engineered hydrogel reveals contribution of matrix mechanics to esophageal adenocarcinoma and identifies matrix-activated therapeutic targets. *J. Clin. Invest.* **133**, e168146 (2023).
74. B. L. LeSavage *et al.*, Engineered matrices reveal stiffness-mediated chemoresistance in patient-derived pancreatic cancer organoids. *Nat. Mater.* **23**, 1138-1149 (2024).
75. N. M. LaMarche *et al.*, An IL-4 signalling axis in bone marrow drives pro-tumorigenic myelopoiesis. *Nature* **625**, 166–174 (2024).
76. A. Hérault *et al.*, Myeloid progenitor cluster formation drives emergency and leukaemic myelopoiesis. *Nature* **544**, 53–58 (2017).
77. A. J. Casbon *et al.*, Invasive breast cancer reprograms early myeloid differentiation in the bone marrow to generate immunosuppressive neutrophils. *Proc. Natl. Acad. Sci. U.S.A.* **112**, E566–E575 (2015).
78. J. Albrengues *et al.*, Neutrophil extracellular traps produced during inflammation awaken dormant cancer cells in mice. *Science* **361**, eaao4227 (2018).
79. L. Borriello *et al.*, Primary tumor associated macrophages activate programs of invasion and dormancy in disseminating tumor cells. *Nat. Commun.* **13**, 626 (2022).
80. N. Linde *et al.*, Macrophages orchestrate breast cancer early dissemination and metastasis. *Nat. Commun.* **9**, 21 (2018).
81. W. Chen, A. D. Hoffmann, H. Liu, X. Liu, Organotropism: New insights into molecular mechanisms of breast cancer metastasis. *NPJ Precision. Oncol.* **2**, 4 (2018).
82. A. Chramiec *et al.*, Integrated human organ-on-a-chip model for predictive studies of anti-tumor drug efficacy and cardiac safety. *Lab. Chip* **20**, 4357–4372 (2020).
83. K. Ronaldson-Bouchard *et al.*, A multi-organ chip with matured tissue niches linked by vascular flow. *Nat. Biomed. Eng.* **6**, 351–371 (2022).
84. P. Carlson *et al.*, Targeting the perivascular niche sensitizes disseminated tumour cells to chemotherapy. *Nat. Cell Biol.* **21**, 238–250 (2019).
85. I. Baldassarri *et al.*, An engineered model of metastatic colonization of human bone marrow reveals breast cancer cell remodeling of the hematopoietic niche. Figshare. https://figshare.com/projects/An_engineered_model_of_metastatic_colonization_of_human_bone_marrow_reveals_breast_cancer_cell_remodeling_of_the_hematopoietic_niche/221386. Accessed 20 September 2024.
86. I. Baldassarri *et al.*, An engineered model of metastatic colonization of human bone marrow reveals breast cancer cell remodeling of the hematopoietic niche. Gene Expression Omnibus. https://www.ncbi.nlm.nih.gov/geo/query/acc.cgi?acc=GSE277786. Deposited 23 September 2024.